Noninvasive measurement of androgen receptor signaling with a positron-emitting radiopharmaceutical that targets prostate-specific membrane antigen

Michael J. Evans[a], Peter M. Smith-Jones[b], John Wongvipat[a], Vincent Navarro[c], Sae Kim[c], Neil H. Bander[c,d], Steven M. Larson[b,e,f], and Charles L. Sawyers[a,g,1]

[a]Human Oncology and Pathogenesis Program, [b]Department of Radiology, [d]Division of Urology, [e]Molecular Pharmacology and Chemistry, [f]Nuclear Medicine Service, and [g]Howard Hughes Medical Institute, Memorial Sloan-Kettering Cancer Center, New York, NY 10065; and [c]Laboratory of Urologic Oncology, Weill Cornell Medical College, New York, NY 10065

Contributed by Charles L. Sawyers, April 28, 2011 (sent for review March 18, 2011)

Despite encouraging clinical results with next generation drugs (MDV3100 and abiraterone) that inhibit androgen receptor (AR) signaling in patients with castration-resistant prostate cancer (CRPC), responses are variable and short-lived. There is an urgent need to understand the basis of resistance to optimize their future use. We reasoned that a radiopharmaceutical that measures intratumoral changes in AR signaling could substantially improve our understanding of AR pathway directed therapies. Expanding on previous observations, we first show that prostate-specific membrane antigen (PSMA) is repressed by androgen treatment in multiple models of AR-positive prostate cancer in an AR-dependent manner. Conversely, antiandrogens up-regulate PSMA expression. These expression changes, including increased PSMA expression in response to treatment with the antiandrogen MDV3100, can be quantitatively measured in vivo in human prostate cancer xenograft models through PET imaging with a fully humanized, radiolabeled antibody to PSMA, ^{64}Cu-J591. Collectively, these results establish that relative changes in PSMA expression levels can be quantitatively measured using a human-ready imaging reagent and could serve as a biomarker of AR signaling to noninvasively evaluate AR activity in patients with CRPC.

Approximately 27,000 patients will die of castration-resistant prostate cancer (CRPC), the lethal form of the disease, in the United States in 2011 (www.cancer.gov). One hallmark of CRPC is reactivation of androgen receptor (AR) signaling despite castrate levels of androgens in the blood (1). This insight has rekindled interest in developing androgen deprivation therapies with greater potency, several of which have already shown clinical activity in patients with CRPC (2–4). Treatment responses, however, are incomplete and short-lived. Given these heterogeneous patterns of response, new biomarkers are urgently needed to document successful AR inhibition in tumor tissue and to identify patients early whose tumors fail to respond.

Serum measurements of the AR-regulated, secreted protein prostate-specific antigen (PSA) are typically used to evaluate AR signaling in prostate cancer. PSA is highly useful for evaluating initial response to androgen deprivation therapies and detecting relapse (5), but reductions in serum PSA levels do not always correlate with survival benefit in CRPC patients. Radiographic studies often demonstrate tumor responses, but these can be mixed, with some lesions shrinking whereas others are stable or expanding, likely a reflection of the heterogeneity of prostate cancer even within the same patient (6). The differential sensitivity of distinct metastatic lesions to antiandrogen therapy might be explained by different levels of AR inhibition. Because declines in serum PSA levels reflect an average across all lesions, it is not currently possible to determine whether AR inhibition varies at different sites.

We reasoned that these difficulties could be overcome with a radiopharmaceutical that measures intratumoral AR signaling. The basis for our optimism extends from previous work demonstrating that molecular imaging tools [e.g., ^{18}F-fluorodeoxyglucose (^{18}F-FDG), ^{18}F-16β-fluoro-5α-dihydrotestosterone (^{18}F-FDHT), ^{11}C-methionine] can capture the biological diversity of CRPC (7–9), in addition to the emerging role of molecular imaging in the evaluation of cancer therapies. For instance, documenting the metabolic tumor response to imatinib with ^{18}F-FDG has greatly simplified the clinical management of gastrointestinal stromal tumors (10, 11).

Although originally identified on the basis of its restricted pattern of tissue expression, prostate-specific membrane antigen (PSMA) emerged as a candidate imaging biomarker of AR activity on the basis of two reports showing that androgen suppresses PSMA expression in the LNCaP prostate cancer cell line (12, 13). Consistent with this observation, Wright et al. (14) reported elevated immunohistochemical staining for PSMA in a small cohort of primary and metastatic biopsies sampled after various androgen deprivation manipulations. Moreover, PSMA is a type II plasma membrane protein expressed abundantly in prostate cancer epithelia, and a substantial catalog of laboratory and clinical imaging tools directed to this protein has been generated (15). Collectively, these observations led us to hypothesize that PET imaging of PSMA might be a viable strategy to measure AR inhibition in vivo.

Results

PSMA Is Androgen Repressed in Multiple Prostate Cancer Models. Prior work implicating PSMA as an androgen-repressed gene is based on a single cell line. To determine whether this biological response is observed more broadly, we surveyed a panel of six prostate cancer cell lines. PSMA is expressed in four AR-positive, hormone-responsive prostate cancer cell lines (LNCaP, CWR22Rv1, LAPC4, and VCaP) but not in two AR-negative prostate cancer lines (PC3 and DU145) or in two immortalized primary prostate epithelial cell lines (BPH and RWPE1; Fig. S1). Androgen stimulation for 72 h with testosterone, 5α-dihydrotestosterone (DHT) or the synthetic AR agonist R1881 reduced PSMA protein levels in cultured LNCaP, CWR22Rv1, LAPC4, and VCaP cells comparedwith the low androgen environment of FBS and the androgen-free envi-

Author contributions: M.J.E., N.H.B., and C.L.S. designed research; M.J.E., P.M.S.-J., J.W., V.N., and S.K. performed research; P.M.S.-J. contributed new reagents/analytic tools; M.J.E., P.M.S.-J., N.H.B., and C.L.S. analyzed data; and M.J.E., S.M.L., and C.L.S. wrote the paper.

Conflict of interest statement: The article describes a new radiotracer to monitor androgen receptor signaling noninvasively. The various studies that demonstrate the utility of this radiotracer include an experiment using the antiandrogen drug MDV3100. C.L.S. is a co-inventor of MDV3100 and owns stock in the company (Medivation) that is developing the drug for prostate cancer treatment. The article does not make any claims about the efficacy of MDV3100; it merely uses it as tool to evaluate the new radiotracer. N.H.B. is the inventor of patents related to PSMA antibodies assigned to Cornell Research Foundation.

Freely available online through the PNAS open access option.

[1]To whom correspondence should be addressed. E-mail: sawyersc@mskcc.org.

This article contains supporting information online at www.pnas.org/lookup/suppl/doi:10.1073/pnas.1106383108/-/DCSupplemental.

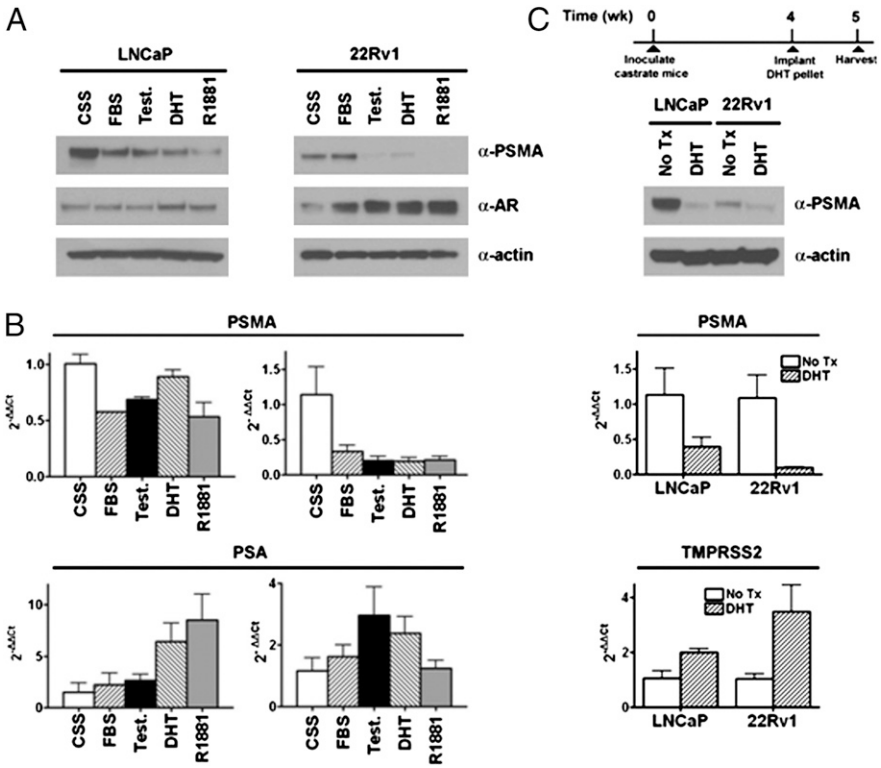

Fig. 1. Androgens suppress PSMA in multiple prostate cancer cell lines and xenografts. (*A*) Incubation of the hormone-responsive prostate cancer cell lines LNCaP and CWR22Rv1 (22Rv1) for 72 h with the endogenous androgens testosterone (Test., 10 nM) and DHT (10 nM) or the synthetic androgen R1881 (0.1 nM) decreases PSMA protein levels compared with low androgen conditions (FBS and CSS). In CWR22Rv1 cells, AR levels increase after androgen treatment compared with vehicle control, suggesting agonist-mediated receptor stabilization and minimal hormone degradation during incubation. (*B*) PSMA mRNA levels are suppressed after 72 h of treatment with androgens in LNCaP and CWR22Rv1, consistent with transcriptional regulation of PSMA by hormone treatment. As anticipated, mRNA levels of PSA, an AR target gene, increase in response to androgen challenge, confirming the bioactivity of hormone treatment at this time point. (*C*) Subcutaneous xenografts of LNCaP and CWR22Rv1 derived in castrate male mice were harvested 7 d after implantation of a DHT pellet or no surgical treatment (No Tx). Immunoblot (*Upper*) and quantitative PCR analysis (*Lower*) shows that PSMA is expressed in PCa xenografts, and expression is reduced by DHT treatment. The androgen-stimulated gene product TMPRSS2 is up-regulated by DHT, confirming the bioactivity of the pellet dose.

ronment in charcoal-stripped serum (CSS) (Fig. 1*A* and Fig. S2). Moreover, PSMA mRNA levels were reduced by androgen treatment in LNCaP (~50% maximal reduction) and CWR22Rv1 (~80% maximal reduction), whereas PSA mRNA levels were elevated, as expected (Fig. 1*B*). These in vitro data confirm that PSMA expression is suppressed by androgens across a panel of AR-positive cell lines. To evaluate hormonal regulation of PSMA in vivo, we established subcutaneous (s.c.) LNCaP and CWR22Rv1 xenografts in castrate male mice. Xenograft tissue harvested and analyzed from mice 7 d after receiving an s.c. DHT pellet showed a substantial reduction in PSMA mRNA and protein levels compared with tissue derived from mice receiving no treatment. As expected, the androgen-stimulated gene TMPRSS2 was up-regulated by DHT treatment (Fig. 1*C*). Collectively, these results show that PSMA is consistently repressed by androgen treatment in multiple prostate cancer models.

AR Is Required for Androgen Repression of PSMA. To confirm that the suppression of PSMA expression by androgen is AR dependent, we ablated AR with siRNA in LNCaP and CWR22Rv1 and subsequently evaluated androgen regulation of PSMA. Whereas silencing AR itself did not seem to impact basal PSMA levels at this time point (72 h), knockdown of AR abolished PSMA repression by DHT in both cell lines (Fig. 2*A*).

This observation suggested that pharmacological inhibitors of AR might antagonize androgen-dependent PSMA suppression. To test this hypothesis, LNCaP-AR cells (parental LNCaP overexpressing wild-type AR) were treated with androgen deprivation, and the effect on PSMA surface expression was assayed by FACS analysis with fluorescently labeled J591, a fully humanized mAb that targets an extracellular epitope of PSMA (16, 17). MDV3100, an experimental antiandrogen developed in castration-resistant models of prostate cancer (18), increased PSMA expression compared with vehicle control after 7 d, with further up-regulation after 14 d (Fig. 2*B*). Incubation in media with CSS alone (androgen deprivation) resulted in larger overall up-regulation of PSMA but only after 14 d. Similar results were observed with parental LNCaP cells (Fig. S3). In CWR22Rv1 cells, MDV3100 treatment (10 μM) antagonized suppression of PSMA by 10 nM testosterone, as did harmol hydrochloride (10 μM), a natural product inhibitor of AR that is not ligand competitive (19) (Fig. S4). In summary, these results document the role of AR in androgen-dependent regulation of PSMA and demonstrate that pharmacologic modulation of AR signaling is faithfully reflected by changes in relative PSMA levels. The fact that PSMA up-regulation was visualized after 7–14 d of androgen deprivation suggests that stable AR knockdown may be required to see similar effects using RNAi targeting AR.

Androgen Repression of PSMA Can Be Quantitatively Imaged with PET. We next explored whether androgen-dependent changes in PSMA expression are sufficiently large to be quantitatively imaged in vivo with PET. To this end, bilateral s.c. CWR22Rv1 xenografts were established in the flanks of castrate male mice and were imaged by PET with ^{64}Cu-J591 (Fig. 3 *A* and *B*). All xenografts had approximately equivalent basal incorporation of ^{64}Cu-J591 [average standardized uptake value $(SUV)_{mean}$ = 39.7 ±

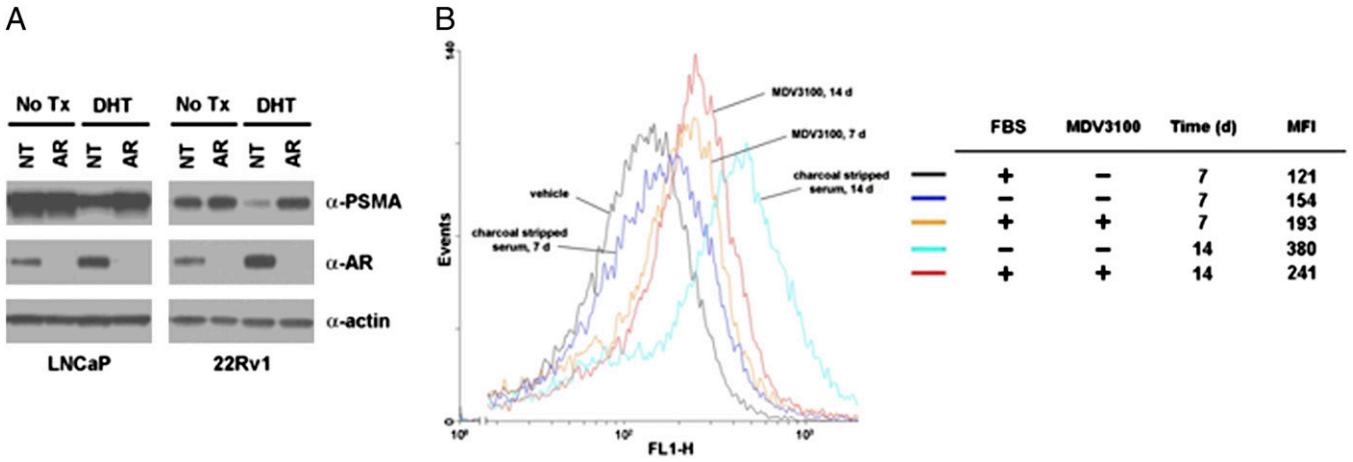

Fig. 2. Genetic and pharmacological inhibition of AR blocks androgen suppression of PSMA. (*A*) LNCaP and CWR22Rv1 (22Rv1) were transfected with nontargeted (NT) or AR-directed (AR) siRNA pools and treated with vehicle (EtOH) or DHT (10 nM). Whereas basal expression of PSMA is unaffected by AR knockdown in either cell line at this time point, AR silencing inhibits PSMA suppression by DHT, thus suggesting a role for AR in this process. Cells were transfected with 100 nM of siRNA, DHT challenge was initiated 24 h after transfection, and cells were harvested 48 h after androgen treatment. (*B*) Hormone withdrawal and antiandrogen treatment increase PSMA expression in LNCaP-AR in vitro. Cells were plated in media containing 10% (vol/vol) FBS and treated with vehicle, MDV3100 (10 μM), or the media was replaced with 10% (vol/vol) CSS (indicated as "-"). After 7 or 14 d, cells were harvested and incubated with Alexa Fluor 488-labeled J591, and PSMA expression was analyzed by FACS. Mean fluorescent intensities (MFI) were calculated and show that MDV3100 up-regulates PSMA expression by 7 d, whereas the effects of hormone withdrawal were observed between 7 and 14 d.

6.5%ID/mL]. Twenty-four hours after imaging, mice were randomized into equal cohorts receiving (*i*) no treatment, (*ii*) a s.c. testosterone pellet, or (*iii*) an s.c. DHT pellet. After 6 d, the groups were again injected with ^{64}Cu-J591, imaged 16 h after injection, and subsequently euthanized for ex vivo tissue analysis. A modest reduction in tumor uptake of ^{64}Cu-J591 was observed 7 d after the initial injection in the group receiving no treatment (0.81 ± 0.08), likely owing to the presence of residual antibody from scan 1. Nevertheless, testosterone and DHT treatments greatly reduced the incorporation of ^{64}Cu-J591 in tumor tissue compared with no-treatment control (0.52 ± 0.1 and 0.45 ± 0.1 respective ratios, $P < 0.01$; Fig. S5 shows a plot of correlated PET and biodistribution data, and Table S1 lists SUV_{mean} and biodistribution data from the tumor tissue of the full mouse cohort). Moreover, biodistribution data revealed that ^{64}Cu-J591 uptake was unaffected in androgen-insensitive host tissues, indicative of specific pharmacological effects of testosterone and DHT (Fig. 3*C*; Table S2 lists biodistribution values from the full mouse cohort).

Androgen Deprivation Therapies Increase ^{64}Cu-J591 Uptake in Xenografts. Having shown that androgen repression of PSMA can be quantitatively imaged, we asked whether up-regulation of PSMA expression can be detected with ^{64}Cu-J591 PET after treatment with antiandrogens. The preclinical studies of MDV3100 were conducted in LNCaP-AR xenografts and were predictive of clinical activity; therefore, we conducted our PSMA imaging studies using the same model. Intact male mice were inoculated with bilateral s.c. LNCaP-AR xenografts, and basal uptake of ^{64}Cu-J591 was determined (average SUV_{mean} = 30.5 ± 9.3%ID/g). Mice were then randomized into cohorts receiving (*i*) vehicle (daily oral gavage), (*ii*) castration, or (*iii*) MDV3100 (daily oral gavage, 10 mg/kg). Tumor volumes decreased by 10–20% 7 d

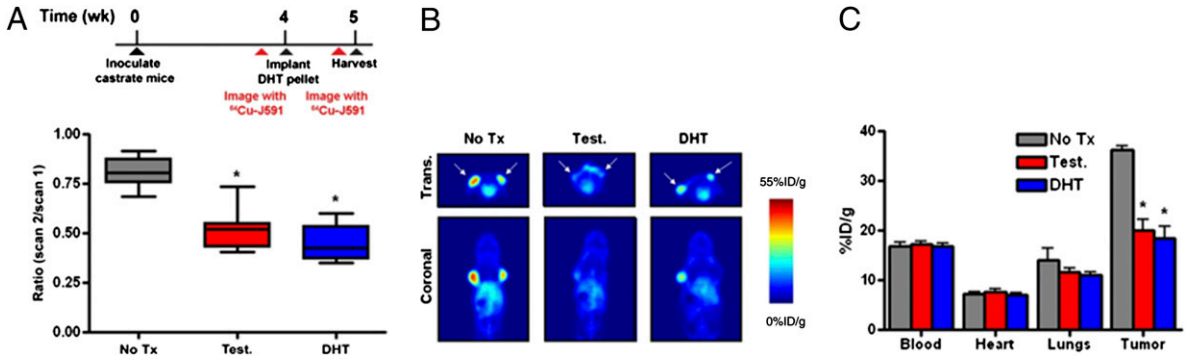

Fig. 3. Detection of androgen repression of PSMA in prostate cancer xenografts by PET. (*A*) Bilateral s.c. CWR22Rv1 xenografts were established in castrate male mice and imaged by PET with ^{64}Cu-J591 24 h before manipulation (scan 1). Animals were again injected with ^{64}Cu-J591 6 d after hormonal manipulation (Test., DHT) or no treatment (No Tx), and scan 2 was acquired 16 h after injection on day 7. The ratio of SUV_{mean} values (scan 2/scan 1) shows substantial reduction in ^{64}Cu-J591 incorporation in the xenografts exposed to testosterone (Test.) and DHT treatment. (*B*) Representative transverse and coronal slices (scan 2) of animals bearing CWR22Rv1 xenografts showing visibly reduced uptake in tumors exposed to androgens compared with no treatment. The positions of the tumors are indicated with arrows. (*C*) Ex vivo biodistribution data (%ID/g) of the tumors and selected host tissues show that the tumors alone, and not androgen-insensitive tissues, respond to hormonal manipulation. Fig. S5 shows a graphical representation of the correlation between calculated SUV_{mean} values and activity measurements acquired ex vivo, Table S1 lists the SUV_{mean} and biodistribution data from the full cohort of mice, and Table S2 lists the activity measurements (%ID/g) from the host tissues. *$P < 0.01$ compared with No Tx controls.

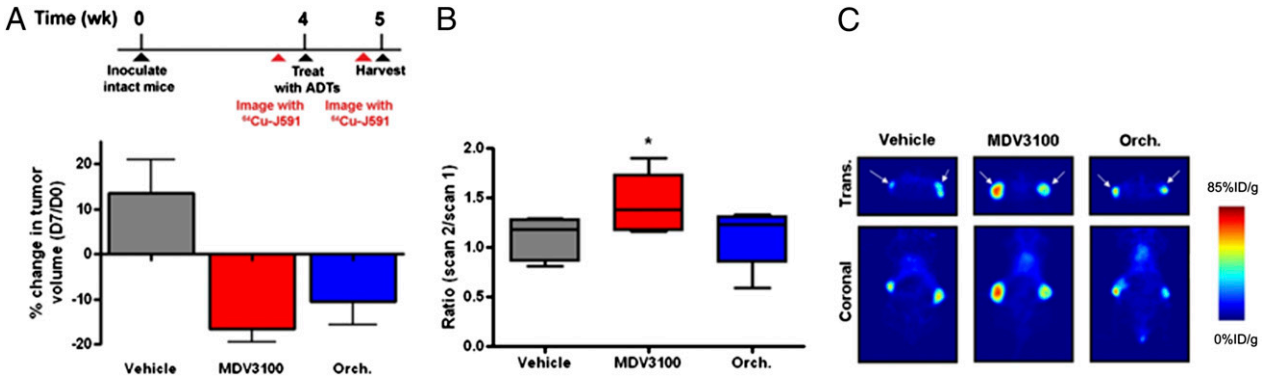

Fig. 4. ^{64}Cu-J591 PET detects up-regulation of PSMA expression in prostate cancer xenografts in response to androgen deprivation therapies. (*A*) Percentage change in tumor volumes show that LNCaP-AR xenografts, established in intact male mice, regress after castration (Orch.) or daily oral gavage of MDV3100 (10 mg/kg). Tumor volume measurements were recorded at day 0 and after the final treatment on day 7. (*B*) To evaluate the effect of antiandrogen therapy on ^{64}Cu-J591 incorporation, mice were imaged 24 h before the initiation of therapy (scan 1), and after 6 d of therapy mice were again injected with ^{64}Cu-J591 and imaged by PET 16 h after radiotracer injection (scan 2). SUV_{mean} values were calculated, and the ratio for each tumor (scan 2/scan 1) is reported. The change in ^{64}Cu-J591 uptake associated with vehicle treatment and castration was minimal, but MDV3100 induced a measurable increase in ^{64}Cu-J591 binding, consistent with the in vitro data. (*C*) Representative transverse and coronal slices (scan 2) of animals bearing LNCaP-AR xenografts showing increased intratumoral uptake of ^{64}Cu-J591 in tumors exposed to MDV3100 compared with castration or vehicle. The positions of the tumors are indicated with arrows. Fig. S5 shows a graphical representation of the correlation between calculated SUV_{mean} values and activity measurements of tumor tissue ex vivo, and Table S3 lists the SUV_{mean} and biodistribution data from the full cohort of mice. ADTs, androgen deprivation therapies. *$P < 0.05$ compared with vehicle.

after castration or MDV3100 treatment, as expected (Fig. 4*A*). After 6 d, the groups were again injected with ^{64}Cu-J591, imaged 16 h after injection, and subsequently euthanized for ex vivo tumor analysis. Whereas the relative change in intratumoral uptake of ^{64}Cu-J591 in cohorts receiving no treatment or castration was minimal (ratios of 1.10 ± 0.2 and 1.13 ± 0.2, respectively), MDV3100 treatment significantly increased the incorporation of ^{64}Cu-J591 in the xenografts compared with vehicle (1.43 ± 0.2, $P < 0.05$; Fig. 4 *B* and *C*; Fig. S5 shows a plot of correlated PET and biodistribution data, and Table S3 lists SUV_{mean} values from the full mouse cohort).

Discussion

Recent clinical success with two next-generation therapies that target AR signaling in CRPC, abiraterone and MDV3100, highlights the importance of developing noninvasive tools to quantitatively monitor the state of AR pathway activity in patients. Despite their promise, responses to these compounds are heterogeneous and often transient. Reasons for treatment failure are unclear. Although changes in serum PSA levels can serve as a surrogate for AR activity, this approach cannot detect variability in response of independent lesions within the same patient. Here we provide proof of concept in clinically validated xenograft models that cell-surface PSMA expression is AR dependent and can be quantitatively assessed by PET using a humanized monoclonal antibody cleared for clinical use.

^{18}F-FDHT, a radioligand that targets the ligand-binding domain of AR, assesses receptor occupancy but not downstream activity. Recent studies of ^{18}F-FDHT PET in CRPC patients treated with MDV3100 found that tumors in nearly all patients showed a decrease in ^{18}F-FDHT binding, indicating that MDV3100 can occupy the AR ligand-binding domain and preclude ^{18}F-FDHT binding. However, these ^{18}F-FDHT PET "responses" did not correlate with declines in serum PSA or tumor response (3). Therefore, ^{18}F-FDHT PET may have utility in optimizing the dose of antiandrogen required for complete blockade of androgen binding to AR, but it cannot assess AR pathway activity. By quantitatively assessing expression of a downstream AR target gene, ^{64}Cu-J591 PET may identify those patients whose tumors retain AR activity despite blockade of the AR ligand-binding domain and therefore would be ideal candidates for additional, orthogonal therapies to fully inhibit AR signaling.

The molecular basis for down-regulation of PSMA expression by AR remains unclear. Noss et al. (12) localized the DHT-mediated suppression of PSMA to an enhancer region, but no androgen response elements have been identified. Recent AR ChIP-Seq reveals four peaks of AR binding among multiple introns of PSMA in LNCaP (20). Functional studies are needed to determine whether these sites mediate AR repression.

The molecular imaging strategy described here could have near-term clinical impact because the unlabeled J591 antibody has already been optimized for use in patients (21, 22). Recent success imaging preclinical prostate cancer models with ^{89}Zr-labeled rather than ^{64}Cu-labeled J591 (23) adds further confidence that this mAb could be readily adapted for a feasibility study in patients. Another clinical implication of our finding that PSMA is up-regulated in response to antiandrogen therapy is that a toxin-conjugated PSMA-targeted mAb could be an effective combination therapy with antiandrogens. Indeed, J591 has been adapted for radioimmunotherapy, and Ab–drug conjugates and therapeutic doses are well tolerated in patients (24, 25).

Materials and Methods

Detailed information is provided in *SI Materials and Methods*.

Antibody Radiolabeling. The monoclonal antibody J591 was modified with 1,4,7,10-tetraazacyclododecane-*N*,*N*′,*N*″,*N*‴-tetraacetic acid (DOTA), by direct coupling of one of the four carboxylic acid groups of DOTA to the primary amines in the antibody protein structure. The antibodies were labeled with ^{64}Cu by adding 10 μL of $^{64}CuCl_2$ to 150 μL of DOTA-J591 (3.3 mg/mL, 1.0 M NH_4OAc), and the solution incubated at 37 °C for 20 min. Twenty-five microliters of 50 mM diethylenetriaminepentaacetic acid (pH 7.0) was added and the solution incubated for an additional 5 min. The reaction mixture was then purified on a 10-mL column of P6 Bio-Gel (Bio-Rad) with an eluant of 1% BSA/saline. The resultant ^{64}Cu-DOTA-J591 had a specific activity of 1.5 GBq/mg (220 MBq/μmol), an immunoreactivity of >90%, and a radiochemical purity of >99.8%.

PET Imaging. Animal studies were carried out under Protocol 06-07-012 approved by the MSKCC Institutional Animal Care and Use Committee. Institutional guidelines for the proper, humane use of animals in research were followed.Bilateral s.c. xenografts of CWR22Rv1 or LNCaP-AR were established in the flanks of castrate or intact male mice, respectively. At tumor volumes of 200 mm^3, the animals were injected with 30 MBq of ^{64}Cu-J591 (20 μg IgG, 200 μL) in the tail vein. After 16 h, the animals were sedated using 1.5% isofluorane (Baxter Healthcare) and imaged with a microPET camera (Concorde Microsystems). Ten-minute acquisitions were collected with an energy window of

350–750 keV, and a coincidence-timing window of 6 ns was used. Twenty-four hours after the initial image, the mice were manipulated (castrates >were treated with an s.c. testosterone or DHT pellet; intacts were castrated or gavaged daily with vehicle or 10 mg/kg MDV3100 for 7 d). After 6 d the mice were injected with ^{64}Cu-J591 and were imaged 16 h after injection. Tumor size was measured twice with calipers, once before initiating treatment and again on day 7. At the end of the last PET scan the animals were euthanized with CO_2. The major organs were removed and counted in a gamma counter with a known sample of the %ID. Region-of-interest analysis of the acquired images was performed using ASIPro software (Siemens Medical Solutions), and the observed maximum pixel value was corrected for partial volume effects according to the size of the tumor and normalized to the injected dose to give the percentage of the injected dose per mL of tumor (%ID/mL).

ACKNOWLEDGMENTS. We thank Valerie Longo and Pat Zanzonico of the Small-Animal Imaging Core Facility at Memorial Sloan-Kettering Cancer Center (MSKCC) for providing technical services and Thomas Voller of Washington University School of Medicine (St. Louis, MO) for the production of ^{64}Cu. The Small Animal Imaging Core Facility was supported by the National Institutes of Health (R24 CA83084 and P30 CA08748); production of ^{64}Cu was supported by the National Institutes of Health (R24 CA86307). M.J.E. was supported by an R25T training grant in molecular imaging (R25-CA096945) from the National Institutes of Health. C.L.S. was supported by the Howard Hughes Medical Institute. S.M.L. and P.M.S.-J. were supported by the Ludwig Center for Cancer Immunotherapy at MSKCC and by National Cancer Institute Grant P50-CA86483. N.H.B., V.N., and S.K. are supported by the David H. Koch Foundation and the Peter M. Sacerdote Foundation.

1. Scher HI, Sawyers CL (2005) Biology of progressive, castration-resistant prostate cancer: directed therapies targeting the androgen-receptor signaling axis. *J Clin Oncol* 23:8253–8261.
2. Chen Y, Sawyers CL, Scher HI (2008) Targeting the androgen receptor pathway in prostate cancer. *Curr Opin Pharmacol* 8:440–448.
3. Scher HI, et al.; Prostate Cancer Foundation/Department of Defense Prostate Cancer Clinical Trials Consortium (2010) Antitumour activity of MDV3100 in castration-resistant prostate cancer: A phase 1-2 study. *Lancet* 375:1437–1446.
4. Reid AH, et al. (2010) Significant and sustained antitumor activity in post-docetaxel, castration-resistant prostate cancer with the CYP17 inhibitor abiraterone acetate. *J Clin Oncol* 28:1489–1495.
5. Lilja H, Ulmert D, Vickers AJ (2008) Prostate-specific antigen and prostate cancer: Prediction, detection and monitoring. *Nat Rev Cancer* 8:268–278.
6. Liu W, et al. (2009) Copy number analysis indicates monoclonal origin of lethal metastatic prostate cancer. *Nat Med* 15:559–565.
7. Meirelles GS, et al. (2010) Prognostic value of baseline [18F] fluorodeoxyglucose positron emission tomography and 99mTc-MDP bone scan in progressing metastatic prostate cancer. *Clin Cancer Res* 16:6093–6099.
8. Larson SM, et al. (2004) Tumor localization of 16beta-18F-fluoro-5alpha-dihydrotestosterone versus 18F-FDG in patients with progressive, metastatic prostate cancer. *J Nucl Med* 45: 366–373.
9. Nuñez R, et al. (2002) Combined 18F-FDG and 11C-methionine PET scans in patients with newly progressive metastatic prostate cancer. *J Nucl Med* 43:46–55.
10. Antoch G, et al. (2004) Comparison of PET, CT, and dual-modality PET/CT imaging for monitoring of imatinib (STI571) therapy in patients with gastrointestinal stromal tumors. *J Nucl Med* 45:357–365.
11. Gayed I, et al. (2004) The role of 18F-FDG PET in staging and early prediction of response to therapy of recurrent gastrointestinal stromal tumors. *J Nucl Med* 45: 17–21.
12. Noss KR, Wolfe SA, Grimes SR (2002) Upregulation of prostate specific membrane antigen/folate hydrolase transcription by an enhancer. *Gene* 285:247–256.
13. Mostaghel EA, et al. (2007) Intraprostatic androgens and androgen-regulated gene expression persist after testosterone suppression: Therapeutic implications for castration-resistant prostate cancer. *Cancer Res* 67:5033–5041.
14. Wright GL, Jr., et al. (1996) Upregulation of prostate-specific membrane antigen after androgen-deprivation therapy. *Urology* 48:326–334.
15. Holmes EH (2001) PSMA specific antibodies and their diagnostic and therapeutic use. *Expert Opin Investig Drugs* 10:511–519.
16. Smith-Jones PM, et al. (2000) In vitro characterization of radiolabeled monoclonal antibodies specific for the extracellular domain of prostate-specific membrane antigen. *Cancer Res* 60:5237–5243.
17. Smith-Jones PM, et al. (2003) Radiolabeled monoclonal antibodies specific to the extracellular domain of prostate-specific membrane antigen: Preclinical studies in nude mice bearing LNCaP human prostate tumor. *J Nucl Med* 44:610–617.
18. Tran C, et al. (2009) Development of a second-generation antiandrogen for treatment of advanced prostate cancer. *Science* 324:787–790.
19. Jones JO, et al. (2009) Non-competitive androgen receptor inhibition in vitro and in vivo. *Proc Natl Acad Sci USA* 106:7233–7238.
20. Yu J, et al. (2010) An integrated network of androgen receptor, polycomb, and TMPRSS2-ERG gene fusions in prostate cancer progression. *Cancer Cell* 17:443–454.
21. Morris MJ, et al. (2005) Pilot trial of unlabeled and indium-111-labeled anti-prostate-specific membrane antigen antibody J591 for castrate metastatic prostate cancer. *Clin Cancer Res* 11:7454–7461.
22. Morris MJ, et al. (2007) Phase I evaluation of J591 as a vascular targeting agent in progressive solid tumors. *Clin Cancer Res* 13:2707–2713.
23. Holland JP, et al. (2010) 89Zr-DFO-J591 for immunoPET of prostate-specific membrane antigen expression in vivo. *J Nucl Med* 51:1293–1300.
24. Bander NH, et al. (2005) Phase I trial of 177lutetium-labeled J591, a monoclonal antibody to prostate-specific membrane antigen, in patients with androgen-independent prostate cancer. *J Clin Oncol* 23:4591–4601.
25. Galsky MD, et al. (2008) Phase I trial of the prostate-specific membrane antigen-directed immunoconjugate MLN2704 in patients with progressive metastatic castration-resistant prostate cancer. *J Clin Oncol* 26:2147–2154.